Transient and steady-state amplitudes of resonant three-dimensional sloshing in a square base tank with a finite fluid depth

O. M. Faltinsen, O. F. Rognebakke, and A. N. Timokha
Centre for Ships and Ocean Structures, NTNU, N-7491 Trondheim, Norway

(Received 14 April 2005; accepted 28 November 2005; published online 25 January 2006)

An adaptive asymptotic nonlinear modal system is used for systematic quantification of three-dimensional steady-state resonant sloshing in a square base tank with a finite fill depth. The depth/breadth ratios are $\geqslant 0.4$. The tank is laterally excited with frequency close to the lowest natural frequency. The main emphasis is on the "swirling" wave regime and its special features, e.g., stability, feedback of higher modes, and regular and irregular switch of the apparent direction of rotation. Theoretical results are validated for both steady-state solutions and "beating" that does not die out in experimental investigations. Frequency domains with no stable steady-state waves and occurrence of "chaotic" waves are discussed. © *2006 American Institute of Physics*.
[DOI: 10.1063/1.2160522]

I. INTRODUCTION

Both horizontal (sway and surge) and angular (roll and pitch) harmonic excitations of a square base tank with frequency σ close to the lowest natural frequency $\sigma_{1,0}$ lead to violent nonlinear three-dimensional waves (sloshing). The literature contains only a few experimental and theoretical studies on the subject. Faltinsen *et al.*[1–3] recognized a note by Stolbetsov,[4] who was probably the first to study this problem theoretically. Arai *et al.*[5,6] performed model tests and isolated Computational Fluid Dynamics (CFD) simulations. They reported rotary waves (called "swirling"), which are well known from the publications on sloshing in upright circular cylindrical or spherical tanks (see experiments by Abramson[7] and appropriate theories by Miles[8] and Gavrilyuk *et al.*[9]). The majority of other publications are devoted to shallow fluid flows (Ockendon *et al.*,[10] Ockendon and Ockendon,[11] and Wu *et al.*[12]), Faraday waves due to vertical excitations (Feng and Sethna,[13] Henderson and Miles,[14] Miles,[15] and Perlin and Schultz[16]), free-standing waves (Bridges[17,18] and Bryant and Stiassnie,[19,20]) and nonresonant excitation, i.e., σ is away of the lowest natural frequency (La Rocca *et al.*[21,22]).

Faltinsen *et al.*[1] studied nonlinear resonant sloshing in a square base basin by assuming an inviscid incompressible fluid with irrotational flow and no overturning of the free surface. Accounting for a dominating character of the two primary excited modes and Moiseyev's asymptotics, they derived a nonlinear modal system coupling the amplitudes of the nine lower modes. This system approximates nonlinear resonant waves in the asymptotic limit $\delta=\sqrt{\delta_1^2+\delta_2^2}\to 0$, where δ_1 and δ_2 are nondimensional horizontal and angular forcing amplitudes, respectively. Steady-state asymptotic solutions of this modal system were obtained for harmonic oscillations of the tank in two distinct forcing planes: parallel to a pair of vertical walls (longitudinal excitations) and diagonal. "Planar" and "diagonal" waves occur in the forcing planes for longitudinal and diagonal excitation, respectively, and two types of three-dimensional wave regimes exist, i.e., "swirling" and "square"-like (also called nearly diagonal). Faltinsen *et al.*[1,3] studied stability of the steady-state regimes and showed that square-like waves are hardly realized for the fluid depth/breadth ratio $h\geqslant 0.4$ and therefore swirling is the sole common three-dimensional wave for excitations in both forcing planes. This has been confirmed by experiments.

However, robust simulations of stable steady-state swirling for the cases tested experimentally were possible only when the initial conditions coincide with those from the asymptotic solutions. Small disturbances relative to δ of these conditions have led to a strong progressive activation of the second-order modes followed by numerical breakdown. Even though the tested nondimensional forcing amplitudes δ were small, i.e., ≈ 0.01 or 1% of the tank breadth for lateral forcing, the numerical failure can possibly be explained by the asymptotic character of the modal system. Indeed, numerical tests confirm that the probability of numerical breakdown increases with δ and, in general, disappears for $\delta<0.001$. Bearing in mind marine applications dealing with amplitudes even up to 10% of the tank breadth and remembering earlier two-dimensional results by Faltinsen and Timokha,[23] Faltinsen *et al.*[2] proposed a modification of the modal system. The altered system accounts for linear viscous damping in dominating modes and matches both Moiseyev's and secondary resonance asymptotics, which are of importance for small, but not infinitesimal, δ. The viscous damping rates have been computed according to Martel *et al.*[24] Some details on the adaptive modal system are presented in the preliminaries of the present paper. Faltinsen *et al.*[2] focused basically on short transient time series. Systematic quantification of steady-state wave amplitudes or hydrodynamic forces and moments versus the forcing frequency has not been performed. The first reason was that clearly periodic signals were not detected in the experiments on a long-time scale due to small damping and local breaking at the walls. The second reason was difficulties in distinguishing long-time transients leading to swirling and irregular motions, because both exhibit the same behavior, which consists of random switching between clockwise and coun-

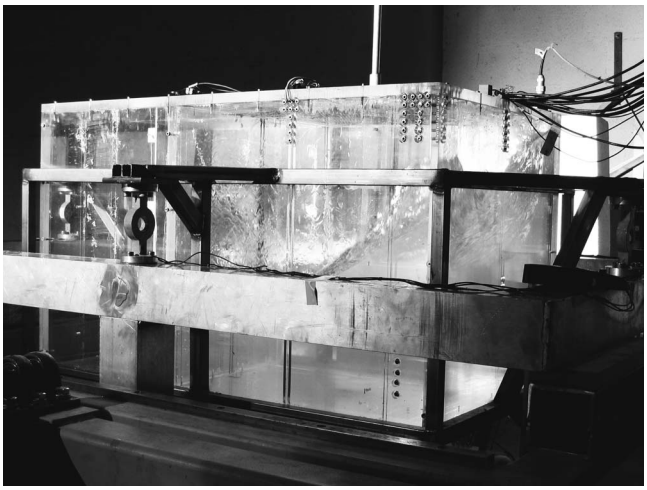

FIG. 1. Image from video recording of swirling for lateral excitation with $\sigma/\sigma_{1,0}=0.988\,41$, $\delta_1=0.016\,34$, $\delta_2=0$, and depth/breadth ratio $h=0.5$ (enhanced online).

terclockwise rotary waves. Irregular motions occur in frequency domains where all the steady-state solutions are unstable. Steady-state and transient waves and the mentioned complications are addressed in the present paper.

Because earlier experimental series were too short to reach steady-state regimes, we performed some longer duration model tests. For "planar" and "diagonal" types of motions, the last seconds of our recordings (after about 100-150 forcing periods) almost always exhibited a periodic behavior so that fluctuations of wave amplitude due to beating are less than δ. The same last seconds for swirling demonstrated a stable rotary wave, but with local breaking and much larger fluctuations of amplitude. The local breaking phenomenon can be seen in the movie in Fig. 1. The variation in amplitude calls for systematic study of transient amplitudes, in general, and typical time periods (phases) characterizing the passage to steady-state solutions, in particular. Due to these tasks, the present paper rejects a variety of path-following procedures that compute periodic solutions of modal systems (see examples by Hermann and Timokha[25] and Ikeda and Ibrahim[26]). This study utilizes long-time numerical series with initial conditions associated with the model tests. The adaptive modal system has relatively small dimension and the direct simulations are CPU efficient. Even for three-dimensional sloshing the required numerical precision was achieved with 27 nonlinear ordinary differential equations of the second order.

Section II gives necessary background and, after a short description of asymptotic results for $\delta\to 0$, states details of adaptive modal modeling by Faltinsen *et al.*[2] Section III discusses earlier and new model tests including observed wave patterns. Important physical factors that are not accounted for by the mathematical model, e.g., local fluid flows at the vertical walls and appearance of overturning free surface, are extensively discussed. Section IV presents comparative results on steady-state and transient amplitudes obtained by adaptive modal theory and experiments. First, the effective frequency domains of both stable steady-state waves and unsteady, irregular motions are found to be in clearly better agreement with experimental findings than documented by Faltinsen *et al.*,[1,3] especially for diagonal excitations and with increasing lateral forcing amplitudes for which ranges of irregular waves are detected. Second, numerical analysis shows that, even though a stable steady-state solution exists, it may not be realized for some model test initial conditions. In these cases, both simulations and experiments clearly demonstrate irregular ("chaotic") behavior. Third, while theoretical amplitudes of stable steady-state diagonal and planar waves are close to the mean arithmetic value of measured data made during the last seconds of model tests, theoretical predictions for swirling solutions imply a lower limit of the mean experimental values. The adaptive modal analysis is able to quantify this point by evaluating transient amplitudes. Transition to stable swirling is shown to include an essential time-period enumerated as Phase III, where rotary waves do not change direction and fluctuation of amplitudes is less than the dominating asymptotic order, but mean amplitude is larger than for the steady-state regime. The existence of this phase can intuitively be related to significant contribution of higher modes due to the secondary resonance (Faltinsen *et al.*[2]). Because passage to swirling is very sensitive to initial conditions and $O(\delta)$-order disturbances of dominating modes significantly increase the duration of phase III, effects of local breaking may be of importance.

II. PRELIMINARIES

A. Statement of the problem

Let a square base tank with base breadth L_1 be partially filled by an incompressible perfect fluid with mean depth h. We assume potential flow and make lengths nondimensional by dividing with L_1, so that the tank breadth and width are equal to 1. A consequence is that values of the physical parameters including $h:=h/L_1$ and $g:=g/L_1$ (g is the gravity acceleration) are redefined so that h in the following text is dimensionless while g has dimension $[s^{-2}]$. Combined prescribed sway/surge and roll/pitch motions of the tank are described by a pair of time-dependent vectors $\dot{\boldsymbol{\eta}}(t)=\boldsymbol{v}_O(t)=[v_{O1}(t),v_{O2}(t),0]$ and $\dot{\boldsymbol{\psi}}(t)=\boldsymbol{\omega}(t)=[\omega_1(t),\omega_2(t),0]$ representing instantaneous translatory and angular velocities of the mobile Cartesian coordinate system $Oxyz$ relative to an absolute coordinate system $O'x'y'z'$ (Fig. 2). The coordinate system $Oxyz$ is rigidly framed with the tank. Its origin O coincides with the middle point of the mean fluid surface, which belongs to the Oxy plane. The Ox and Oy axes are parallel to the vertical walls.

The free boundary problem on fluid sloshing is based on a series of physical idealizations implying, in particular, the absence of overturning waves and reads

$$\Delta\Phi=0 \quad \text{in } Q(t); \quad \frac{\partial\Phi}{\partial\nu}=\boldsymbol{v}_O\cdot\boldsymbol{\nu}+\boldsymbol{\omega}\cdot[\boldsymbol{P}\times\boldsymbol{\nu}] \quad \text{on } S(t),$$

$$\frac{\partial\Phi}{\partial\nu}=\boldsymbol{v}_O\cdot\boldsymbol{\nu}+\boldsymbol{\omega}\cdot[\boldsymbol{P}\times\boldsymbol{\nu}]+\frac{f_t}{\sqrt{1+(\nabla f)^2}} \quad \text{on } \Sigma(t); \quad \int_{Q(t)}dQ=\text{const},$$

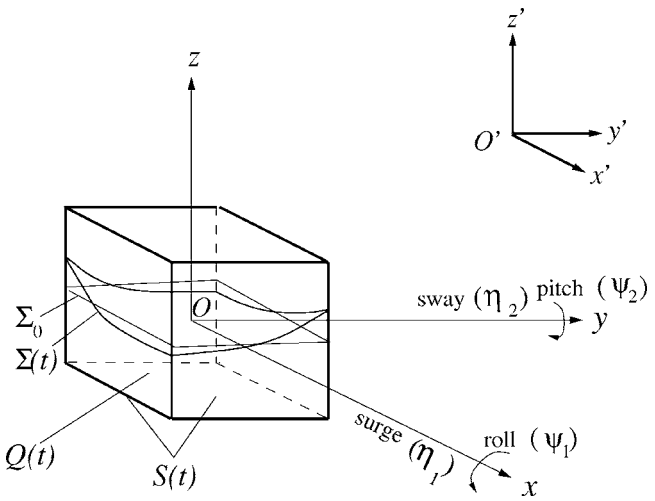

FIG. 2. Sketch of a square base tank forced in sway/surge and roll/pitch. Rigid body motions are considered in the moving coordinate system $Oxyz$ framed with the rigid tank.

$$\frac{\partial \Phi}{\partial t} + \frac{1}{2}(\nabla \Phi)^2 - \nabla \Phi \cdot (\boldsymbol{v}_O + \boldsymbol{\omega} \times \boldsymbol{P}) + U = 0 \quad \text{on } \Sigma(t). \tag{1}$$

Here the unknowns are the function $f(x,y,t)$ defining the free surface evolution $\Sigma(t): z=f(x,y,t)$ and the absolute velocity potential $\Phi(x,y,z,t)$, which should be calculated in time-varying volume $Q(t)$ confined to the wetted body surface $S(t)$ and $\Sigma(t)$; $\boldsymbol{\nu}$ is outward normal to $Q(t)$. The gravity potential U depends on the spatial coordinates (x,y,z) and time t, namely, $U(x,y,z,t)=-\boldsymbol{g}\cdot\boldsymbol{P}', \boldsymbol{P}'=\boldsymbol{P}'_O+\boldsymbol{P}$, where $\boldsymbol{g}$ is the gravity acceleration vector and the absolute position vector $\boldsymbol{P}'(t)=(x',y',z')$ can be decomposed into the sum of $\boldsymbol{P}'_O(t)=O'O$ and the relative position vector $\boldsymbol{P}=(x,y,z)$ (see Fig. 2).

The evolutional free boundary problem (1) should be completed by either initial or periodicity conditions. The initial (Cauchy) conditions require

$$f(x,y,t_0) = f_0(x,y), \qquad \left.\frac{\partial \Phi}{\partial \nu}\right|_{\Sigma(t_0)} = V_0(x,y) \tag{2}$$

to be known at $t=t_0$. Solutions of (1) and (2) correspond to transient waves. When $\dot{\boldsymbol{\eta}}(t)$ and $\dot{\boldsymbol{\psi}}(t)$ are periodic with the forcing period T, the periodicity condition

$$f(x,y,t+T) = f(x,y,t), \qquad \nabla \Phi(x,y,z,t+T) = \nabla \Phi(x,y,z,t) \tag{3}$$

implies steady-state wave motions.

Finding a solution of (1) and (3) and computing $f(x,y,t_0)$ and $\partial\Phi/\partial\nu$ on $\Sigma(t_0)$ determine initial boundary conditions, which lead to periodic solutions of (1).

B. Asymptotic predictions for small-amplitude resonant forcing

When $\boldsymbol{v}_O=\boldsymbol{\omega}=\boldsymbol{0}$, the linear sloshing problem (Faltinsen *et al.*[1]) has the fundamental solutions $\Phi = \exp(I\sigma_{i,j}t)\varphi_{i,j}(x,y,z)$ $(I^2=-1)$, where the natural modes $\varphi_{i,j}$ are computed by

$$\varphi_{i,j}(x,y,z) = f_{i,j}(x,y)\frac{\cosh[\lambda_{i,j}(z+h)]}{\cosh(\lambda_{i,j}h)},$$

$$f_{i,j}(x,y) = \cos\left[\pi i\left(x-\frac{1}{2}\right)\right]\cos\left[\pi j\left(y-\frac{1}{2}\right)\right],$$

$$\lambda_{i,j} = \pi\sqrt{i^2+j^2}, \quad \sigma_{i,j}^2 = g\lambda_{i,j}\tanh(\lambda_{i,j}h), \quad i,j \geqslant 0,$$

$$i+j \neq 0, \tag{4}$$

and $\sigma_{i,j}$ are the natural frequencies. Projections of $\varphi_{i,j}$ on the mean free surface $z=0$ define shapes of standing waves $\{f_{i,j}(x,y)=\varphi_{i,j}|_{z=0}, i+j\geqslant 1\}$ that constitute an appropriate Fourier basis in the square cross section. The functions $\{\varphi_{i,j}(x,y,z), i+j\geqslant 1\}$ form a complete system of harmonic functions in the unperturbed fluid domain $Q_0=[-1/2,1/2]\times[-1/2,1/2]\times[-h,0]$, which satisfies zero-Neumann boundary conditions on the wetted tank surface.

The modal technique by Faltinsen *et al.*[1,28] suggests the free surface elevation $z=f(x,y,t)$ to be presented in the tank-fixed $Oxyz$-coordinate system as

$$f(x,y,t) = \sum_{i+j\geqslant 1}^{\infty} \beta_{i,j}(t) f_{i,j}(x,y), \tag{5}$$

where the time-dependent modal functions $\beta_{i,j}(t)$ are unknown *a priori*. This representation does not admit overturning waves and assumes vertical tank walls in the free surface zone. Substituting (5) into the original nondimensional free boundary problem (1) or its variational analogy (Faltinsen *et al.*[28] and La Rocca *et al.*[22]) yields a multidimensional system of nonlinear ordinary differential equations (modal system) in $\beta_{i,j}$. The modal system using truncated (5) implies additional limitations to instantaneous surface shapes including requirement of right contact angles at the vertical walls and run up in terms of thin films of water at the walls. The modal technique makes it possible to account for damping and, in its multidimensional form, for amplification of higher modes.

Let us now assume that the external forcing is a harmonic function, i.e., $\dot{v}_{Oi}=-\sigma^2\epsilon_i\cos\sigma t$, $\dot{\omega}_i=-\sigma^2\varepsilon_{0i}2\pi\cos\sigma t$, $i=1,2$, with

$$\epsilon_1 = \delta_1\cos\theta, \quad \epsilon_2 = \delta_1\sin\theta, \quad \varepsilon_{01} = \delta_2\cos\theta,$$

$$\varepsilon_{02} = \delta_2\sin\theta. \tag{6}$$

$\delta_1 \ll 1$ is the nondimensional amplitude of translatory excitation, δ_2 is the nondimensional angular amplitude, and $(\cos\theta, \sin\theta)$ is the unit guiding vector of the excitations. The resulting small nondimensional amplitude for the combined horizontal and angular excitations can be defined as

$$\delta = \sqrt{\delta_1^2+\delta_2^2} \ll 1. \tag{7}$$

Using the modal technique based on the representation (5) and the appropriate modal system utilizing the third-order Moiseyev ordering,

$$\beta_{i,j} = O(\delta^{1/3}), \quad i+j=1; \quad \beta_{i,j} = O(\delta^{2/3}),$$
$$i+j=2; \quad \beta_{i,j} \leqslant O(\delta), \quad 3 \leqslant i+j, \tag{8}$$

Faltinsen *et al.*[1,3] found the asymptotic periodic solutions, which describe the steady-state resonant waves for $\sigma \to \sigma_{1,0} = \sigma_{0,1}$. The lowest-order terms of these asymptotic solutions are

$$\beta_{1,0}(t) = A\cos\sigma t + \bar{A}\sin\sigma t + O(\delta);$$
$$\beta_{0,1}(t) = \bar{B}\cos\sigma t + B\sin\sigma t + O(\delta), \tag{9}$$

where $A, \bar{A}, B, \bar{B} = O(\delta^{1/3})$. The dominating amplitudes $A, \bar{A}, B, \bar{B}$ are governed by a system of nonlinear algebraic equations [Faltinsen *et al.*,[1] Eq. (3.10)], which does not always have a solution and may have multiple solutions.

The case of longitudinal forcing ($\varepsilon_{O2} = \epsilon_2 = 0$ or $\theta = 0$) is characterized by three and only three types of asymptotic solutions (9) that take the following form:

(i) planar waves:

$$f(x,y,t) = Af_{1,0}(x)\cos\sigma t + O(\delta);$$
$$\bar{A} = B = \bar{B} = 0, \tag{10}$$

(solution implies two-dimensional sloshing in the plane of excitation);

(ii) square-like waves:

$$f(x,y,t) = [Af_{1,0}(x) \pm \bar{B}f_{0,1}(y)]\cos\sigma t + O(\delta);$$
$$\bar{A} = B = 0 \tag{11}$$

[here, $|A| \neq |B|$ and (11) corresponds to a nearly diagonal standing wave, but $\pm$ implies the possibility that the waves can occur approximately along either of the two diagonals]; and finally,

(iii) swirling waves:

$$f(x,y,t) = Af_{1,0}(x)\cos\sigma t \pm Bf_{0,1}(y)\sin\sigma t + O(\delta); \quad \bar{B} = \bar{A} = 0. \tag{12}$$

The reason why (12) describes swirling is that the x- and y-dependent terms are 90° out of phase. The $\pm$ ahead of amplitude component B in (12) means clockwise or counterclockwise rotary waves. Initial conditions and the transient phase will determine the direction. Because both signs are possible in (11) and (12), (i)–(iii) imply not three but five different solutions.

The case of diagonal excitation leads to the same square-like sloshing, but

(i*) diagonal waves,

$$f(x,y,t) = A[f_{1,0}(x) \pm f_{0,1}(y)]\cos\sigma t + O(\delta) \tag{13}$$

[$\pm$ for $\theta = \pi/4$ or $3\pi/4$ in (6), respectively] occurs instead of the planar (i) and another structure for

(iii*) swirling waves,

$$f(x,y,t) = (A\cos\sigma t \pm B\sin\sigma t)f_{1,0}(x) + (A\cos\sigma t \mp B\sin\sigma t)f_{0,1}(y) + O(\delta), \tag{14}$$

with $|A| \neq |B| A \neq 0$, $B \neq 0$. One should note that, although (14) also determines a rotary wave, it is not equivalent to (12). The sign in (14) depends on initial conditions. One obvious fact is that the x- and y-dependent terms are never 90° out of phase. The phase shift is also not zero and depends exclusively on A and B, namely, is a function of the forcing parameters. Analogously to the case of longitudinal forcing, we have five distinct steady-state solutions.

Studying (i)/(i*), (ii), and (iii)/(iii*) for different h, δ, and σ makes it possible to establish the frequency domains where different types of resonant waves are stable. By assuming a multitiming technique, Faltinsen *et al.*[1,3] estimated these effective frequency domains in the asymptotic limit $\delta \to 0$. The results are in satisfactory agreement with model tests. In particular, both experiments and theory show that square-like waves are not realized for $h \geqslant 0.4$. These are either unstable or coexist with (i)/(i*), but have a much larger energy. Numerical and experimental studies show that, as a rule, the wave system with smallest energy appears when different steady-state waves coexist.

Another important discovery consists of frequency domains where all of the three steady-state wave regimes are unstable. Bearing in mind the possibility of chaos in those domains, we called them "chaotic." Similar domains for sloshing in an upright circular cylindrical tank are presented in applied mathematical studies by Miles[8] and Funakoshi and Inoue.[27] The dual steady-state solutions, first of all swirling, render difficult identification of chaotic domains from the experimental data. The reason is that dual solution switching in transient phase can wrongly lead to conclusion of a chaotic domain.

C. Adaptive modal modeling by Faltinsen *et al.* (Ref. 2)

Pursuing third-order asymptotic theories (see, for instance, the third-order equations by Zakharov[29] for free-standing waves),

$$\beta_{i,j} \sim R_{i,j} = O(\delta^{1/3}), \quad i+j \geqslant 1. \tag{15}$$

Faltinsen *et al.*[1] derived the following infinite-dimensional modal system coupling $\beta_{i,j}$:

$$\sum_{a+b\geqslant 1} \ddot{\beta}_{a,b}\left[\delta_{ia}\delta_{jb} + \sum_{c+d\geqslant 1}\left(d^{1,(i,j)}_{(a,b),(c,d)}\beta_{c,d} + \sum_{e+f\geqslant 1} d^{2,(i,j)}_{(a,b),(c,d),(e,f)}\beta_{c,d}\beta_{e,f}\right)\right] + \sigma^2_{i,j}\beta_{i,j}$$
$$+ \sum_{a+b\geqslant 1}\sum_{c+d\geqslant 1}\dot{\beta}_{a,b}\dot{\beta}_{c,d}\left(t^{0,(i,j)}_{(a,b),(c,d)} + \sum_{e+f\geqslant 1} t^{1,(i,j)}_{(a,b),(c,d),(e,f)}\beta_{e,f}\right) + P^{(2)}_{i,j}[\dot{v}_{O2} + S^{(2)}_j\ddot{\psi}_1 + g\psi_1]$$
$$+ P^{(1)}_{i,j}[\dot{v}_{O1} - S^{(1)}_i\ddot{\psi}_2 - g\psi_2] = 0, \quad i+j \geqslant 1, \tag{16}$$

where all the coefficients are calculated explicitly as func-

tions of h in the Appendix of the paper by Faltinsen *et al.*[1] An advantage of the modal modeling based on (16) is the fact that the hydrodynamic force can easily be found in terms of $\beta_{i,j}$ (see the Appendix).

The system (16) needs the initial conditions

$$\beta_{i,j} = \alpha^0_{i,j}, \quad \dot{\beta}_{i,j} = \alpha^1_{i,j}, \quad i+j \geqslant 1, \tag{17}$$

where the known constants $\alpha^0_{i,j}$ and $\alpha^1_{i,j}$ describe initial fluid shape and the initial velocity, respectively. These constants may be obtained from Fourier treatment of (2). Solutions of (16) and (17) describe transient waves.

For periodic forcing we can also employ the periodicity conditions [equivalent to (3)]

$$\beta_{i,j}(t+T) = \beta_{i,j}(t), \quad \dot{\beta}_{i,j}(t+T) = \dot{\beta}_{i,j}(t), \quad i+j \geqslant 1, \tag{18}$$

where T is the forcing period. Solutions of (16) and (18) describe steady-state wave motions.

The modal technique makes it possible to account for linear viscous damping (Miles[8] and Faltinsen *et al.*[3]) in the framework of analytical estimates of the damping rates by Keulegan,[30] Hill,[31] and Martel *et al.*[24] The modification of the modal system (16) suggests inclusion of the linear terms $2\alpha_{i,j}\dot{\beta}_{i,j}$, where the damping rates $\alpha_{i,j} = \alpha^{\text{surface}}_{i,j} + \alpha^{\text{bulk}}_{i,j}$ were computed in Faltinsen *et al.*[3] as follows:

$$\alpha^{\text{surface}}_{i,j} = \sqrt{\frac{\nu\sigma_{i,j}}{2}}\left[\frac{3}{2} + \frac{\lambda_{i,j}}{\sinh(2\lambda_{i,j}h)}\left(\frac{1}{2} - h\right)\right] \tag{19}$$

(damping due to shear stress on the internal tank surface),

$$\alpha^{\text{bulk}}_{i,j} = 2\nu\left[\left(\frac{\pi^4(ij)^2}{\lambda^2_{i,j}} + \lambda^2_{i,j}\right) + \frac{2h}{\lambda_{i,j}}\frac{\pi^4(ij)^2 - \lambda^4_{i,j}}{\sinh(2\lambda_{i,j}h)}\right] \tag{20}$$

(damping in the fluid bulk). Here, $\nu := \nu/L_1^2$ is the scaled kinematic viscosity.

Formulas (19) and (20) assume $\lambda_{i,j} = O(1)$, which is true only for the lower natural modes. Estimates of damping for higher modes are still an open question, because both experiments and direct numerical simulations based on fully dissipative models establish a nonlinear damping character. In addition, damping of higher modes may be affected by breaking waves.

Faltinsen *et al.*[2] showed that resonant excitations with small but not infinitesimal δ can lead to amplification of higher modes. The Moiseyev ordering (8) should in that case be replaced. Solutions based on (8) may coexist (in the same frequency domain) with solutions based on the secondary resonance asymptotics. In order to match both types of asymptotic solutions and transients between them by a single nonlinear modal system, Faltinsen *et al.*[2] proposed the adaptive ordering

$$\begin{aligned} &\beta_{i,j} = O(\delta^{1/3}), \quad i+j \leqslant N; \quad \beta_{i,j} = O(\delta^{2/3}), \\ &N+1 \leqslant i+j \leqslant 2N; \quad \beta_{i,j} \leqslant O(\delta), \quad 2N+1 \leqslant i+j. \end{aligned} \tag{21}$$

As a consequence, the infinite-dimensional modal system (16) transforms to a finite-dimensional structure by neglecting the terms of $o(\delta)$.

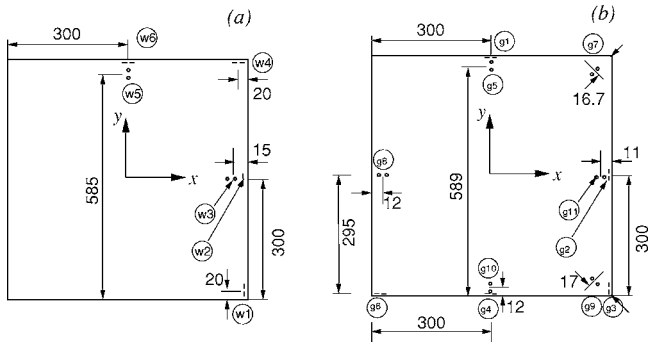

FIG. 3. Top views of the cubic tanks with wave probes for the first (a) and the second (b) model test series.

By increasing N in (21), we get a set of "embedded" modal systems, where the case $N=1$ corresponds to the Moiseyev's modal theory. The number N, which defines dominating modes, is usually not *a priori* known. It can vary with σ and type of steady-state wave regime. A way to find this number consists of testing results obtained with N and $N+1$. If N is consistent with dominating modes, results obtained with N and $N+1$ should differ only by $O(\delta)$. Due to this asymptotic treatment of the convergence, the evaluation of the modal functions that are $O(\delta)$ is unnecessary and therefore the adaptive modal systems can be restricted to the modal functions $\beta_{i,j}$, $1 \leqslant i+j \leqslant 2N$.

The adaptive modal modeling suggests an "adaptive" strategy for the damping of lower and higher modes. While the modal equations associated with the dominating modes $\beta_{i,j}$, $i+j \leqslant N$ are characterized by the damping rates (19) + (20), the second-order modes $i+j \geqslant N+1$ are critically damped, i.e., $\alpha_{i,j} = \sigma_{i,j}$. Faltinsen *et al.*[2] have proved that the error of the adaptive damping strategy has a maximum of $O(\delta)$ that is consistent with the global accuracy of the adaptive modal modeling.

III. EXPERIMENTS

A. Setup

Experiments for sway and roll harmonic excitations were performed in addition to the model tests by Faltinsen *et al.*[1,2] A cubic tank with dimensions 0.6 m has been used. It was filled with fresh water at room temperature. The tank walls are made of 20 mm thick acrylic with a steel frame added for support. The weight of the empty tank and frame is 124 kg. The measurements were within 1 mm of the given values and the tank model was horizontal within 0.5°. Instrumentation consists of wave probes, force gauges, accelerometers, steering system velocity feedback monitoring, and a digital video camera.

The location of wave measuring sensors is shown in Fig. 3. w1, w2, w4, w6 and g1, g2, g3, g4, g6 denotes parallel copper tape fixed to the wall for the first and second session, respectively. Sensors w3, w5 and g5, g7, g8, g9, g10, g11 consist of two lengths of parallel wire stretched vertically between the tank bottom and roof. The wires have a diameter of 0.6 mm and the center distance is around 10 mm and 14 mm. Both types of wave probes, copper tape and wires,

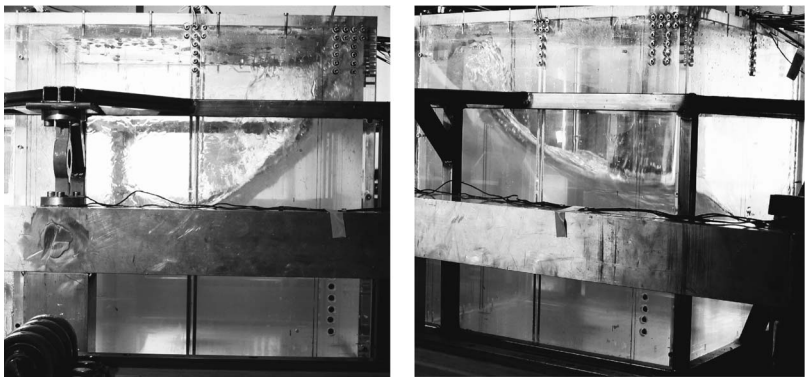

FIG. 4. Local phenomena in the corner during swirling.

are capacitance probes. Because of the surface tension, the wire probes have the accuracy of the order of the wire diameter, in this case 0.6 mm when the instantaneous free surface, except the meniscus, is perpendicular to the wires. If the free surface is steep or curved, the accuracy may be lower. The copper tape probes fixed to the tank walls have accuracy limited by local effects between the free surface and tank wall, exemplified by thin films of water that stick to the wall a short while after the free surface has come down. The copper tape measurements show a high sensitivity to local jet flow at the intersection between the free surface and the tank wall.

Four force gauges referred to as guide towers support the frame enclosing the tank model. Each guide tower includes three strain gauges and facilitate force measurements along all three axes. The accelerometers are aligned with the x and y axes and are situated on top of the tank model. These are used to measure the tank motion, and are a supplement to the measured servomotor velocity from the feedback steering system. The data analysis is performed in Matlab. A filtering frequency of 5 Hz is applied for both forces and accelerations when accelerometer readings are used to calculate the horizontal forces excluding the inertia force due to tank mass. A zero-crossing analysis of the tank motion provides the exact forcing frequency. Fourier analysis of the forced motions has been conducted. It shows that the mechanical system including the servomotor actuators provides a very accurate sinusoidal acceleration. The lowest frequency disturbing the prescribed regular motion is around 9 Hz. This is considered to be sufficiently far away from the input frequency of around 1 Hz. A special damping device was used to reduce the time between each test. A horizontal mesh of metal was lowered onto and through the free surface to suppress the free surface motion. Both earlier and new model tests were performed with fill level 30 cm. The minimum forcing amplitudes were 47 mm for sway/surge and 0.1 rad for roll motions.

B. Experimental steady-state waves

After approximately 2 min or about 120 forcing periods of transient phase, model tests showed either "almost periodic" waves, whose types and frequency domains (Faltinsen *et al.*[3]) are generally consistent with theoretical steady-state predictions (i/i*), (ii), and (iii/iii*), or irregular, chaotic behavior. The duration of transients from zero-initial state to almost periodic regime generally agrees with the damping rates (19) and (20) computed for the primary excited modes (0,1) and (1,0).

When the experiments show steady-state waves, the fluctuation of wave amplitudes and hydrodynamic forces is smaller than the dominating order $O(\delta^{1/3})$, usually in the range between $O(\delta^{2/3})$ and $O(\delta)$. For planar and diagonal waves, the fluctuation is typically $O(\delta)$, but for swirling it is larger, $O(\delta^{2/3})$. Besides, experimental swirling exhibits steep wave patterns, local breaking at the walls, and irregular fluctuation of the recorded wave amplitudes. The standing wave breaking appears as a thin vertical jet, which overturns and forms droplets falling under gravity on the underlaying free surface. Analogous experimental observations were reported by Taylor[32] and Royon *et al.*[33] While occurrence of local run-up and water films covering the vertical walls should not significantly affect the hydrodynamic forces, a focus on the measured wave elevations slightly away from the wall at the sensors w3, w5 and g5, g7, g8, g9, g10, g11 is most robust.

Steep wave profiles indicate considerable amplification of higher modes. The irregular amplitude fluctuation in almost periodic swirling regime can in part be explained by the three-dimensional wave breaking, which is mostly localized at the tank corners as shown in Fig. 4. Although, in contrast to initial transients and irregular motions, the local breaking involves insignificant water mass, falling droplets may cause non-negligible irregular perturbations of higher modes, randomize damping, and thereby extend the transient phase. The literature does not give reliable strategies on how to model the irregular damping fluctuation and disturbances associated with it.

Finally, one should note that our instrumentation does not capture rotational fluid flow (associated with generation of vorticity) due to swirling as documented by Royon *et al.*[33] for a circular base basin. However, observations indicate that local rotational flows are generated in the corners of the square base tank.

IV. RESULTS AND DISCUSSION

A. Adaptive modal modeling of transition to a steady-state regime

1. Steady-state amplitudes

Description of response curves for stable steady-state solutions and comparison with experiments are the primary

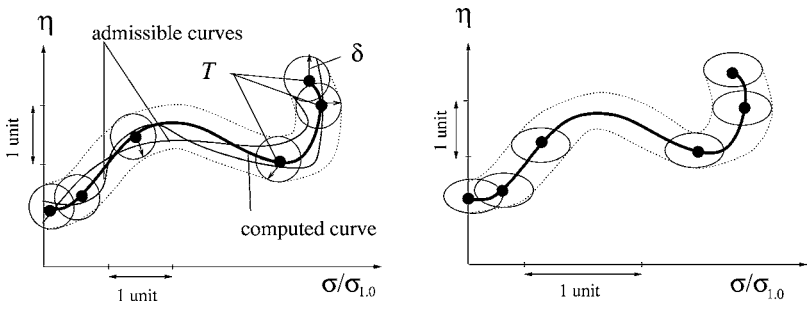

FIG. 5. Computed steady-state response curves by the adaptive modal technique in the $(\sigma/\sigma_{1,0}, \eta)$ plane (bold solid lines, T is an arbitrary point on the curve), where η is either wave amplitude or hydrodynamic force amplitude. Accuracy of the adaptive method is $O(\delta)$ and therefore the actual response curves belong to a $O(\delta)$ neighborhood of the computed data visualized as circles or ellipses depending on the ratio between the axes units.

goals of this section. The adaptive modal system is used to compute a steady amplitude η of wave elevation as well as the hydrodynamic force. Accuracy of the computations is $O(\delta)$. In turn, because the detuning asymptotics are $(\sigma/\sigma_{1,0})^2-1=O(\delta^{2/3})$ for (8) and $(\sigma/\sigma_{1,0})^2-1=O(\delta^{1/2})$ for the secondary resonance, the estimate by the adaptive modal system for $\sigma/\sigma_{1,0}$ is also given to within $O(\delta)$. This means that each point $T=(\sigma/\sigma_{1,0}, \eta)$ on the computed response curves is associated with an admissible circle of $O(\delta)$ radius. Experimental steady-state amplitudes should target a domain formed by the set of these circles moving along the numerical response curves as demonstrated in Fig. 5. The circles are replaced by ellipses when the units of the horizontal and vertical axes are unequal.

A straightforward method for computing response curves consists of treating adaptive modal systems together with the periodicity condition (18) that leads to a two-point boundary value problem. Example of such a numerical study for a two-dimensional sloshing problem was recently given by Hermann and Timokha[25] by using the RWPM package developed to compute parametrized two-point boundary value problems. However, this and similar packages are not applicable to solve tasks of the present paper, because they generally do not allow for stability analysis and description of transient amplitudes. Under these conditions, direct numerical integration of the adaptive modal system with appropriate initial conditions should be the best way to find stable steady-state waves, compute steady parameters η, and describe the experimental transients. Because the adaptive modal systems are of relatively small dimension, these are very CPU efficient so that different initial conditions and related transients can be tested. A limitation of the adaptive modal systems is nonadequate simulation of local phenomena, which are of special importance for complex transients and irregular flows in the frequency domains where there are no stable wave solutions.

2. Transient amplitudes

The startup conditions in the experiments suggest a weakly perturbed free surface implying small initial values of $\beta_{i,j}(0), \dot{\beta}_{i,j}(0)$ relative to δ. Long simulations with this scenario lead to either steady-state (periodic) solution or exhibit irregular, chaotic motions. The transients pass through a maximum of five relatively long time intervals (enumerated as phases I–V), where distinct wave behavior is displayed.

Phase I usually lasts about 30–40 forcing periods. Faltinsen *et al.*[2] studied this phase and established a good agreement with experiments. If there are no stable steady-state solutions, the experiments demonstrate considerable breaking waves, which reduce the agreement to 10-15 forcing periods. Further, both simulations and experiments show that phase I is followed by strongly irregular waves (phase II) that last up to tex forcing periods for transition to planar and diagonal regimes and up to 30–40 forcing periods preceding swirling. Faltinsen *et al.*[2] showed that transients of phase II cannot be precisely approximated by the adaptive method. It is unlikely that any CFD method can accurately describe phase II, because the fluid flow in this time period is very sensitive to small disturbances. Small variations of damping rates, increasing dimension of adaptive systems, and even $O(\delta)$ variations of initial conditions influence the duration and sloshing behavior in phase II. All of these disturbance factors as well as minor physical factors including breaking phenomena bring to mind the saying of "gentle touches to a stone rolling down a mountain can be decisive in determining its future trajectory."

If the modal system describes transition to swirling, phase II is followed by phase III of considerable duration. However, phases III (IV) are absent for planar and diagonal cases. Beginning from phase III, the numerical swirling does not change rotation direction and is characterized by a modulation with a fixed beating period. This is exemplified in Fig. 6. The duration of phase III as well as the maximum (M) and minimum (m) amplitude values may be influenced by the time history at phase II, which is determined by initial conditions. Another deciding factor is the dimension of the adaptive modal system, i.e., the feedback of higher modes and the total damping. However, the arithmetic mean values of m and M remain stable. Note that prolonged calculations with $N \geqslant 5$ become stiff and numerically tedious so that we were not able to study this problem in detail for very large dimensions. This mean value (upper dotted line in Fig. 6) is clearly larger than the steady-state amplitude (lower dotted line).

The next typical time period, phase IV, is characterized by increasing beating periods of modulated waves as well as a monotonic decrease of the mean amplitude. This beating period stabilizes only in phase V where the mean amplitude becomes close to the steady-state value. The duration of phase IV is very sensitive to small variations of the damping, feedback of higher modes to the dominating ones, and $O(\delta)$ disturbances of dominating modal functions $\beta_{i,j}, i+j \leqslant N$. The latter effect can even force the system into phase III.

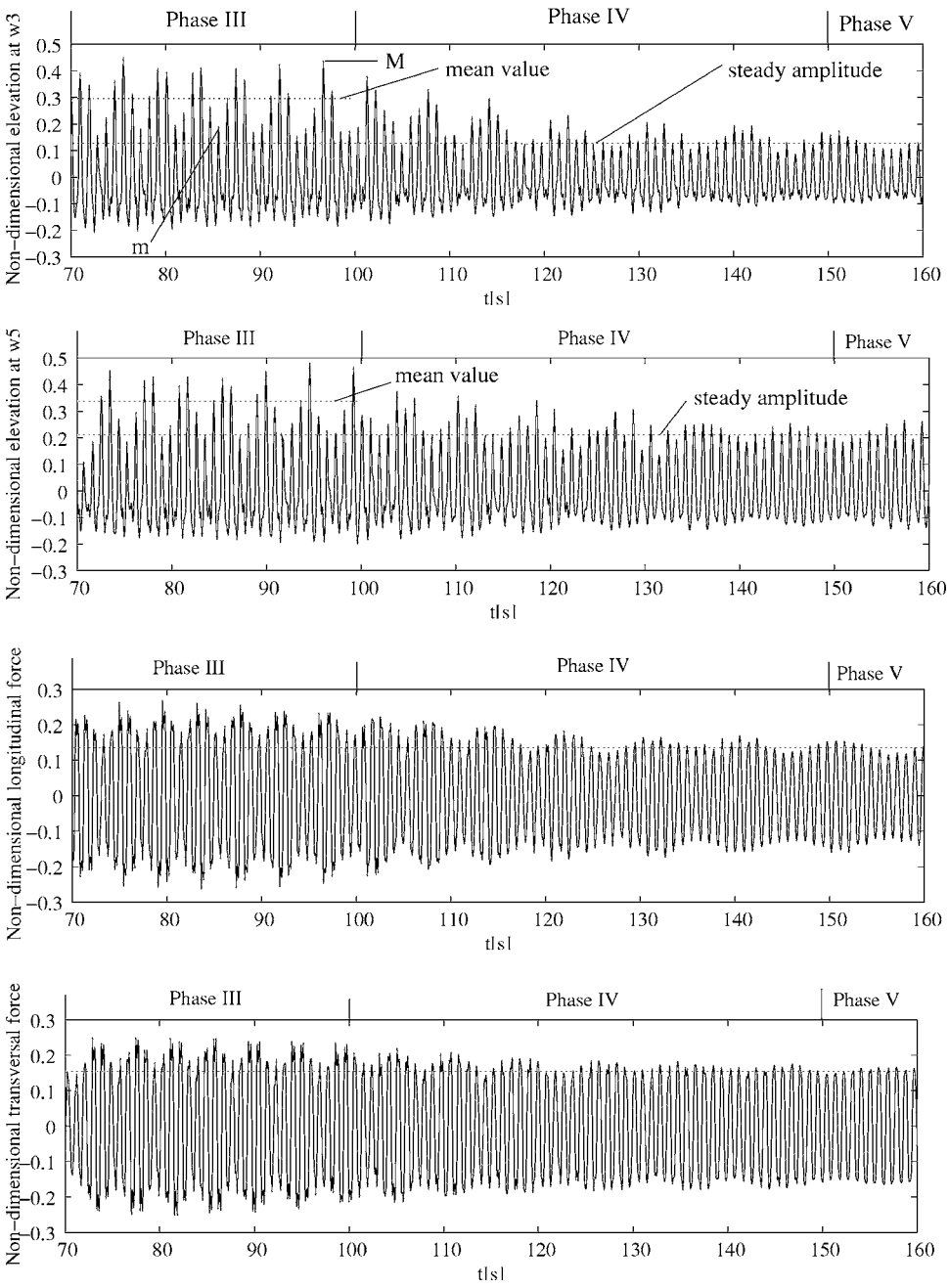

FIG. 6. Transition to steady-state swirling, phases III–V. Nondimensional wave amplitudes (at w3 and w5) and hydrodynamic forces (normalized by $\mathcal{M}L_1$, where $\mathcal{M}$ is the fluid mass). Numerical data for $h=0.5$, $\delta_1=0.008\,17$, $\delta_2=0$, and $\sigma/\sigma_{1,0}=0.99$ (forcing period is 0.9247 s). The lower dotted line represents the steady-state amplitude, and M and m are maximum and minimum amplitudes at phase III, whose mean value is marked by the upper dotted horizontal line.

This indicates the importance of physical imperfections. Finally, after approximately 3000-5000 forcing periods, calculations give steady-state solutions.

The presence of phases III and IV is the principal difficulty for experimental validation of the numerical results. Although swirling is stabilized beginning from phase III, it is not possible to determine from the model test measurements if the current phase is III, IV, or V. The task to distinguish between the transient phases fails even though the difference between maximum and minimum of measured wave amplitudes is small.

B. Response curves for diagonal excitation

Consider the diagonal horizontal harmonic forcing ($\delta_2=0$, $\delta_1\neq 0$) with the unit guiding vector $(1/\sqrt{2},\ 1/\sqrt{2})$ [$\theta=\pi/4$ in (6)]. Theoretical expectations on steady-state regimes by Faltinsen *et al.*[3] consist of stable diagonal and swirling motions as well as chaotic waves in the frequency domain where both of these are unstable. The diagonal regime is characterized by symmetric wave patterns relative to the forcing plane $y=x$ and therefore wave elevations at probes at w3 and w5 are synchronized. Steady amplitudes

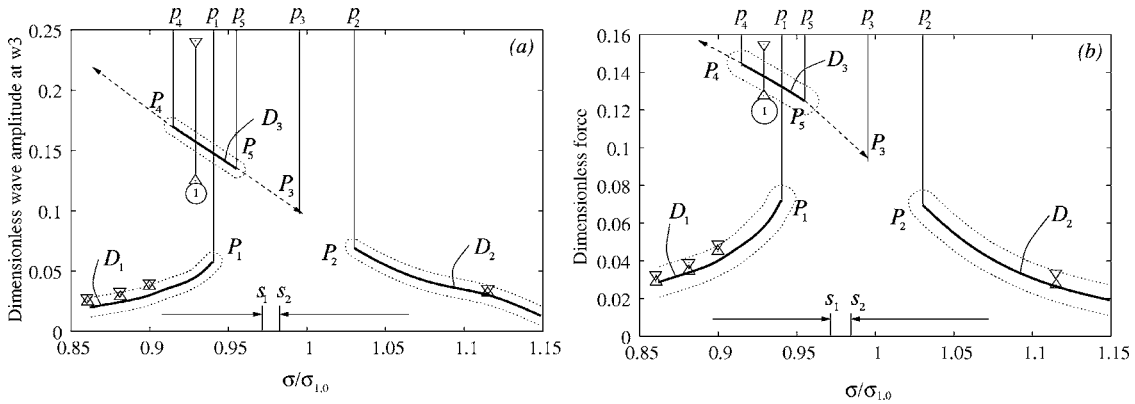

FIG. 7. Diagonal resonant excitations with $h=0.5$, $\delta_1=0.008\,17$, $\delta_2=0$. Response curves for stable diagonal waves. Solid lines (curves D_1, D_2, and D_3) imply theoretical steady-state wave amplitude (dimensionless elevation at w3) and hydrodynamic forces F_x and F_y (normalized by $\mathcal{M}L_1$, where $\mathcal{M}$ is the fluid mass) vs $\sigma/\sigma_{1,0}$. Measured amplitudes are represented by minimum ($\triangle$) and maximum ($\triangledown$) during the last 20 s of the model tests. The figure includes the dotted lines that encompass the δ domains for the expected measured steady-state amplitudes. Points P_i and their abscissas $p_i, i\neq 3$ denote the endpoints of the theoretical response curves, where the diagonal regime changes stability properties. The dashed line shows extra sub-branches, which exist in the asymptotic limit $\delta\to 0$, but disappear in adaptive modal modeling. Analogously, the range (s_1,s_2) implies theoretical estimate of irregular, chaotic motions as $\delta\to 0$.

measured at w3 and w5 and hydrodynamic forces along the Ox and Oy axes should be equal ($\max|F_x|=\max|F_y|$). For swirling, although the asymptotic prediction (14) provides equal amplitudes at w3 and w5 for the $O(\delta^{1/3})$ terms, the higher-order terms [Eqs. (3.8) by Faltinsen *et al.*[1]] display the $O(\delta)$ difference. Similarly, the maximum hydrodynamic forces $|F_x|$ and $|F_y|$ differ by $O(\delta)$. The difference between symmetric (relative to the forcing plane $y=x$) wave elevations for swirling, which implies a pair of dual steady-state solutions, means in particular dependence of $|F_x|$ and $|F_y|$ on the direction of rotation. The direction of swirling depends on the initial conditions and transient perturbations and therefore model tests may selectively demonstrate different directions for the same forcing parameters. Thus, a nondimensional amplitude is introduced, which is the maximum of amplitudes at w3 and w5. Further, the hydrodynamic force amplitude is defined as $F=\max(|F_x|,|F_y|)$.

1. Diagonal waves

Results on steady-state amplitudes for diagonal waves are validated by experiments in Fig. 7. Computations detect two branches D_1 and D_2 of lower amplitude occurring in frequency domains left of p_1 and right of p_2, respectively, and the branch D_3 responsible for diagonal waves of larger amplitude with the effective frequency domain (p_4,p_5). The branches are surrounded by a dotted border, $O(\delta)$ neighborhood, which yields the domain for theoretically admissible amplitudes. This is because the adaptive systems provide approximation of points on $D_i, i=1,2,3$ to within $O(\delta)$. Numerical analysis shows that branches D_1 and D_2 are well approximated with $N=1$ and the difference between the steady-state predictions with $N=2$ is less than δ. This means that secondary resonance phenomena are unimportant for solutions on D_1 and D_2. The situation changes for D_3, where the asymptotic convergence is only established for $N=3$. This explains the difference between the new results and the single-dominant theory. The latter results are formally drawn by the dashed line.

Theoretical results in Fig. 7 were obtained by combining direct simulations with small initial conditions applicable for internal points of D_1 and D_2, and path following along the branches. The latter suggests a stepwise change in forcing frequency and use of the earlier numerical periodic solution for computing new initial conditions at t_0. The path-following procedure corresponds to an artificial model test where the forcing frequency changes very slowly to avoid considerable transients. D_3 was generally obtained by path following after a single numerical series with small initial conditions for $\sigma/\sigma_{1,0}$ in a middle point of (p_1,p_5). Similar series for $\sigma/\sigma_{1,0}<p_1$ always lead to solutions on D_1. The endpoints P_4 and P_5 of D_3 were also detected by path following. Their existence is in particular conflict with results by Faltinsen *et al.*[1] [see Fig. 12, (a) point E is equivalent to P_3] based on single-dominant inviscid model. The latter predicts the corresponding branch for any $\sigma/\sigma_{1,0}\leqslant p_3$ instead of $p_4\leqslant\sigma/\sigma_{1,0}\leqslant p_5$. The new left bound p_4 is most probably associated with damping, but the right bound p_5 is due to amplification of higher modes (convergence requires $N\geqslant 3$). Abscissas of P_1 and P_2, which were also determined by path following, are generally consistent with Faltinsen *et al.*[1] [see Fig. 12, (a) points T and B].

Numerical results are compared with measurements of wave amplitudes during the last 20 s of a total model test duration of 360 s. Maximum and minimum of measured amplitudes are denoted by the pairs of inverted triangles in Fig. 7. Solutions on D_1 and D_2 show very good agreement between theory and experiments. The point ① ($\sigma/\sigma_{1,0}=0.929$) from the model test implies considerable beating, but the mean measured amplitude is close to D_3, especially for the hydrodynamic force. This is because local wave steepness at the walls that cannot be precisely captured by modal approximations.

2. Swirling

Figure 8 completes Fig. 7 by results on swirling occurring inside the range (p_1,p_2). The theoretical steady-state

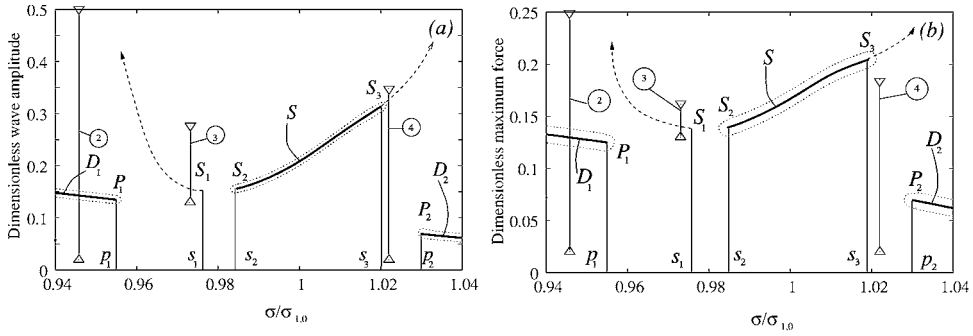

FIG. 8. The same as in Fig. 7, but for swirling. Solid lines (curves D_2 and D_1) are parts of branches in Fig. 7. The curve S with endpoints S_2 and S_3 corresponds to stable swirling, so that (s_2, s_3) is its effective frequency domain. Dashed lines present additional frequency domains of stable swirling established by single-dominant theory [Faltinsen *et al.* (Ref. 3)]. However, adaptive modal theory expects irregular, chaotic motions in the ranges (p_1, s_2) and (s_3, p_2).

amplitude of stable swirling based on the adaptive modal system is represented by the solid line S, which determines the effective frequency domain (s_2, s_3). The dashed lines give the shapes of response curves on swirling in the asymptotic limit $\delta \to 0$ (Faltinsen *et al.*[3]). Path following is used to detect positions of the endpoints S_2 and S_3, where swirling becomes unstable. The abscissa of S_2 is generally consistent with abscissa of the Hopf-bifurcation point established by Faltinsen *et al.*[1] [see Fig. 12(a), the point F_2], but the frequency domain (s_3, p_2) of irregular motions is a novelty caused by complex amplification of higher modes and damping. Besides, swirling left of s_1 is also unstable within the framework of adaptive modal modeling.

In the case of Fig. 8, there are only three test runs in our model tests around the interesting frequency domain (points ②, ③ and ④). All these runs were unfortunately done away from (s_2, s_3) and therefore do not demonstrate swirling but rather irregular, chaotic motions. Very useful is ④ that confirms the mentioned novel zone of hydrodynamic instability between s_3 and p_2. The irregular waves at ②, where a diagonal wave is expected, are easily explained by the initial scenario of the experiments. In this case, path following to the right along D_1 indeed identifies a stable diagonal regime, but calculations with small initial conditions lead to chaotic motions appearing as a perpetual switching swirling direction. Test ③ has been extensively discussed by Faltinsen *et al.*[2] (see Fig. 13). In this case, the model test demonstrates swirling with relatively small fluctuation of the amplitude between 90 and 200 s, but after 200 s the fluctuation increases (see the recordings in Fig. 9) and leads to the conclusion of hydrodynamic instability.

3. Experiments by Faltinsen et al. (Ref. 1)

In order to (i) validate the effective frequency domain of swirling related to the branch S, (ii) confirm chaotic motions in the frequency domain (p_1, s_2), and (iii) show that the zone (s_3, p_2) may disappear for smaller forcing amplitudes, the model test case with diagonal forcing by Faltinsen *et al.*[1] was used. These experiments were of relative short duration (up to 120-160 forcing periods), but the expected types of steady-state motions are clearly identified. Using denoting from Figs. 7 and 8, the theoretical branches D_i, $i=1,2,3$, and S are compared with measured amplitudes during the last 20 s in Fig. 10. Three model tests (points ⑥, ⑦ and ⑧), which imply stable swirling, validate the branch S if the admissible $O(\delta)$ neighborhood marked by the dotted line is accounted for. The model test ⑤ demonstrates irregular motions and thereby confirms instability ranges embedded between S and D_1 and D_3. Finally, for this forcing amplitude, which is slightly lower than in Fig. 7, the adaptive theory does not find instability between S and D_2.

Analysis of measured amplitudes for swirling concludes that measurements ⑧ are most probably made in the numerically found phase V, which has been discussed in Sec. IV A 2. The reasoning is that the mean amplitude is close to

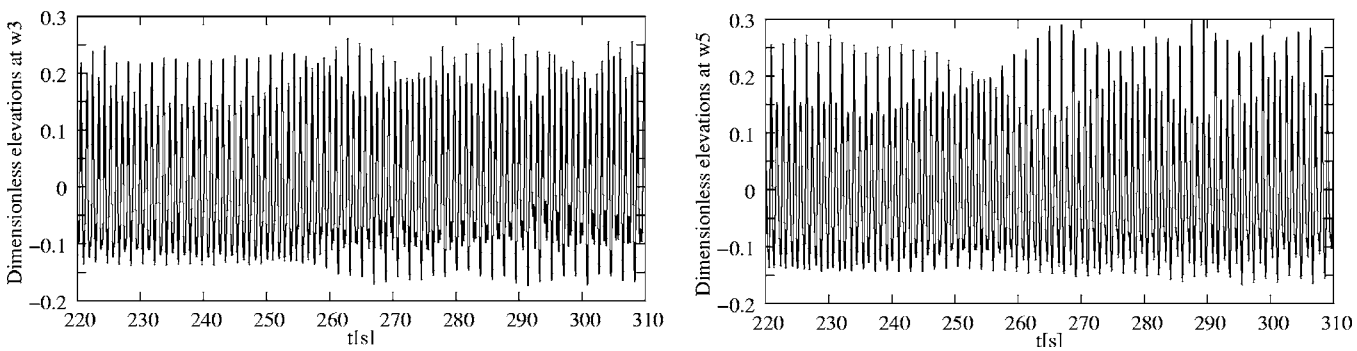

FIG. 9. The last seconds from model test recordings at w3 and w5. Diagonal forcing with $h=0.5$, $\delta_1=0.008\,17$, $\delta_2=0$, and $\sigma/\sigma_{1,0}=0.973$.

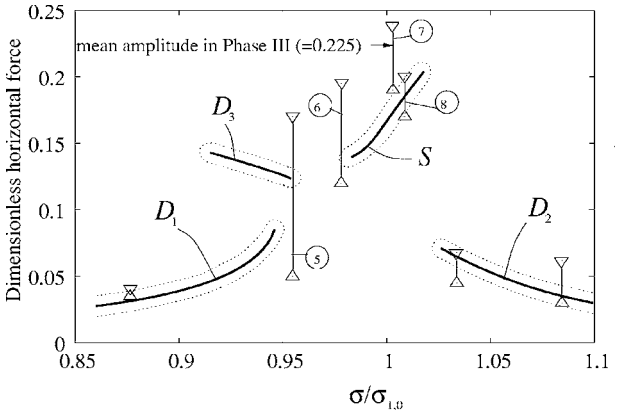

FIG. 10. Theoretical results and model test data on amplitudes of stable steady-state motions. Dimensionless horizontal force consists of maximum of F_x and F_y. Diagonal forcing with $h=0.508$, $\delta_1=0.007\,80$, $\delta_2=0$. The notation is the same as in Figs. 7 and 8.

S. The mean amplitude is larger than the steady-state prediction for ⑥ and ⑦, which indicates that they belong to phase III or IV. This hypothesis has been confirmed by computing mean amplitude in phase III for ⑦. This dimensionless value is equal to 0.225 and clearly larger than the mean value measured at the last 20 s.

C. Response curves for longitudinal excitation

Longitudinal excitation of the tank in Figs. 3(a) has been performed in the *Oxz* plane, but (b) was forced in the *Oyz* plane. Both series were done with the same forcing amplitude. The sensors w and g are situated at slightly different distances from the wall, but we found it acceptable to assume that measurements of wave elevations at w3 and g10 as well as w5 and g8 are similar. The difference in horizontal position is only 3 mm (0.5% of the tank breadth).

1. Surge excitation

Comparison of the theoretical results and experimental data are presented in Fig. 11. Solid lines represent theoretical amplitudes of stable steady-state regimes, but inverted triangles give upper and lower bound of the model test data from the last 20 s of measurements. The adaptive modal technique detects only two types of motions: planar (branches P_1 and P_2) and swirling (branch S_1). Stable square-like wave regimes, which should appear over and to the left of P_1 within the framework of the Moiseyev asymptotics (Faltinsen *et al.*[1]), are not established. Similar as for diagonal excitations, the effective frequency domain of swirling (s_1,s_2) is lower than expected by Faltinsen *et al.*[1,3] and an additional zone of hydrodynamic instability (s_2,p_2) is detected. The effective frequency domain for planar motions generally agrees with earlier predictions.

The agreement between theory and experiments for the effective frequency domains is very good. Measured amplitudes are also well approximated for planar regimes. The model tests (⑨-⑫) that exhibit swirling are both characterized by a significant amplitude fluctuation and give much larger results than the theoretical steady-state predictions. This fact as well as differences of the experimental data for approximately the same forcing parameters (⑨-⑩) imply that measurements probably correspond to phases III-IV so that mean model test amplitudes should be between the mean amplitudes at phase III and the steady amplitude. The mentioned mean amplitudes were computed and drawn as the branch S_2

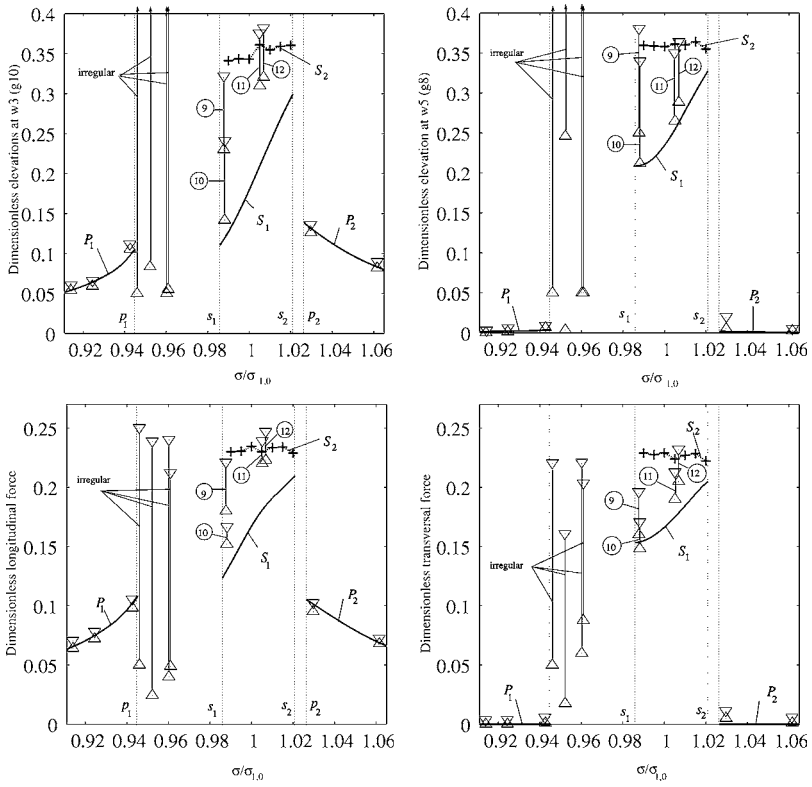

FIG. 11. Longitudinal resonant excitation with $h=0.5$, $\delta_1=0.008\,17$, $\delta_2=0$. Response curves and model test data. Solid lines (curves P_1, P_2, and S_1) imply theoretical steady-state wave amplitude (dimensionless elevation at w3/g10 and w5/g8) and hydrodynamic forces F_x and F_y (normalized by $\mathcal{M}L_1$, where $\mathcal{M}$ is the fluid mass) vs $\sigma/\sigma_{1,0}$. The frequency domains (p_1,s_1) and (s_2,p_2) correspond to irregular, chaotic wave motions. The mean amplitudes in phase III are computed and drawn as the branch S_2 (crest-and-dotted line). Measured amplitudes are represented by minimum (△) and maximum (▽) during the last 20 s of the model tests. Swirling cases are ⑨–12.

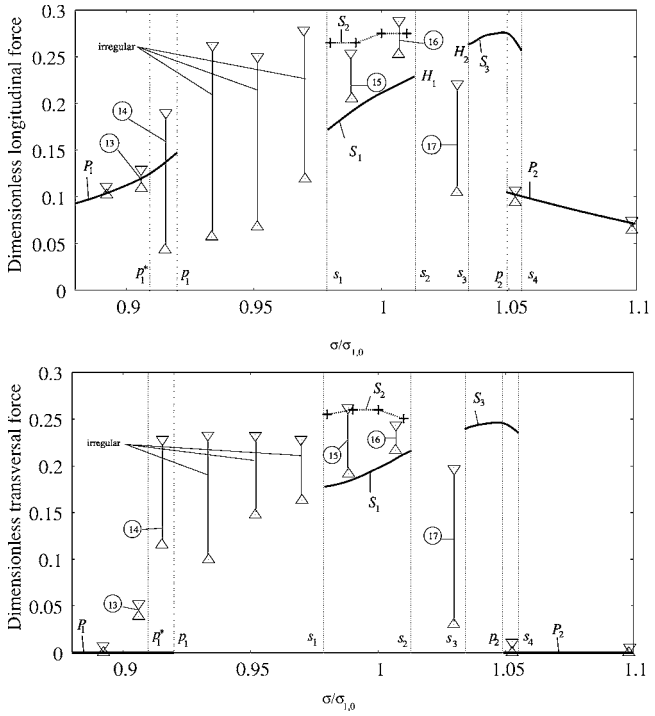

FIG. 12. The same as in Fig. 11, but for $\delta_1=0.016\,34$. The frequency domains (p_1,s_1) and (s_2,s_3) imply theoretical estimates of irregular, chaotic wave motions. The estimate of p_1 changes to p_1^*, if calculations are made with small initial conditions. Swirling cases are 15 and 16.

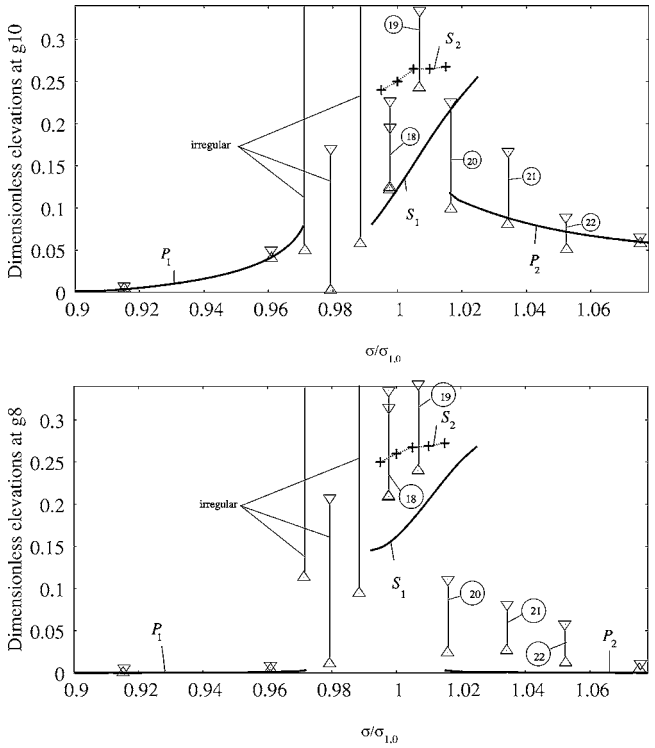

FIG. 13. The same as in Fig. 11, but only for dimensionless wave elevations at g10 and g8 and for roll excitation corresponding to $\delta_1=0.0005$, $\delta_2=0.007\,957\,7$.

(crest-and-dotted line). Figure 11 shows that mean measured amplitudes are really located between S_1 and S_2.

Doubling the forcing amplitude (in our experiments $\delta_1=0.016\,34$, $\delta_2=0$) leads to considerable local wave breaking, which hits the wave probes. This may lead to unpredictable recordings for wave elevation at the walls and makes questionable a good agreement between theoretical results and measurements. A perception about the local phenomena can be obtained from the video recording in Fig. 1. However, because the local phenomena give little influence on integral hydrodynamic characteristics including forces and moments on the tank, the adaptive modal technique should model them adequately. This is confirmed by the results in Fig. 12 (notations are the same as in the case of Fig. 11), where a formal disagreement is only established for model test case 14. The disagreement consists of theoretical expectations of planar waves for $\sigma/\sigma_{1,0}<p_1$ and $\sigma/\sigma_{1,0}>p_2$, but the model test shows clear irregular motions for a duration of at least 5 min. The situation that appeared is similar to case ② for diagonal forcing, where small initial conditions as in the scenario from the experiments prevented realization of the steady-state regime. This means that the value p_1 computed by means of path following along the branch P_1 does not coincide with the actual right bound $\sigma/\sigma_{1,0}<p_1^*$ of the planar regime estimated by direct simulations with small initial conditions. Another test case, 13, is very close to the limit p_1^* and therefore experiments demonstrate very long three-dimensional transients lasting for about 3 min, before reaching planar motions. The experiments stopped after 10 min, but planar motions still showed considerable transversal components.

The main consequence of increasing excitation amplitudes consists of changing the effective frequency domain for stable swirling. It includes two intervals (s_1,s_2) and (s_3,s_4) corresponding to the branches S_1 and S_3, respectively. The zone (s_2,s_3) corresponds to an extended domain (s_2,p_2) in Fig. 11 and implies chaotic waves. Model test 17 confirms the last fact. The effective domain of swirling (s_1,s_2) is validated by experiments 15 and 16, but there is no appropriate model test to validate domain (s_3,s_4). Finally, branch S_2 corresponding to the mean amplitude at phase III justifies the conclusion that mean amplitudes of swirling must lie between S_1 and S_2.

2. Angular excitation

Some model tests with the tank in Fig. 3(a) were performed with small-amplitude harmonic roll excitations with $\delta_1=0.000\,05$ and $\delta_2=0.007\,957\,7$. These can be used to study decreasing excitation amplitude. Theoretical and experimental results are presented in Fig. 13. There is a satisfactory agreement between predicted and measured effective frequency domains. Because this forcing amplitude is small relative to lateral cases in Figs. 11 and 12, the effective frequency domains for planar and swirling are very close to asymptotic predictions by Faltinsen *et al.*[1] This includes the absence of an irregular wave motion zone between the branches S_1 and P_2 and a decrease of the domain between P_1 and S_1. However, these model test cases are characterized by decrease of the total damping, and, as a consequence, by longer transients. These experiments were also performed for up to 300 forcing periods. Evaluating theoretical and mea-

sured wave amplitudes confirms this point for both planar and swirling regimes. For swirling, the prolonged transients clarify different measured maximum wave elevation in model tests 18, which are done with equal forcing. Besides, the wave amplitudes in 19 are significantly higher than for the theoretical steady-state represented by points on the branch S_1 and the measurements were most probably made in the beginning of phase III. The planar cases 20–22 demonstrate that the transversal wave components remain nonsmall during the last 20 s of the model tests.

V. CONCLUSIONS

The present paper quantifies steady-state and transient wave amplitudes and lateral hydrodynamic force of three-dimensional resonant sloshing in a square-base tank. The tank is laterally excited with frequencies close to the lowest natural frequency. The fluid depth/breadth ratio is $\geqslant 0.4$. New and earlier experimental results are used to validate the theory. The main emphasis is on swirling as the most prominent hydrodynamic phenomenon and on small but noninfinitesimal forcing amplitudes δ. The experiments show steep wave profiles and the classical Moiseyev asymptotics (Faltinsen *et al.*[1,3]) may fail to predict steady-state amplitudes responses for this forcing. The nonlinear adaptive modal system is used (Faltinsen *et al.*[2]). It shows good performance and robustness on a long-time scale with arbitrary initial conditions. The simulations are not affected by numerical damping and the results are in good agreement with experiments, especially for hydrodynamic forces. However, there is a shortcoming in modeling the damping of higher modes and feedback of local phenomena of random nature. This is extensively discussed in the validation of theoretical results.

The paper numerically studies the transition to the swirling steady-state regime and its typical phases. Understanding of this process is facilitated by results on mean transient amplitudes for two-dimensional sloshing by Hill[31] and observation of perpetual beating in model tests with swirling. When the calculations use small initial conditions according to the experiments, the transition to swirling detects irregular motions in phases classified as I and II. Eventually, the direction of rotation stops changing, and a long time period (phase III) follows in which a modulated wave with considerably amplified higher modes exists. Fluctuation of the transient amplitudes in phase III is smaller than the dominating order $O(\delta^{1/3})$, but the arithmetic mean amplitude is larger [comparable with $O(\delta^{1/3})$] relative to the steady amplitude detected only after phase V. The modulated wave increases the beating period in the intermediate phases IV and V, but the mean amplitude tends to the steady-state prediction and is equal at phase V. Phases III-V are very long and simulations may increase due to random $O(\delta)$ disturbances that exist in practice due to local breaking at the walls. An indirect validation of the transient phases III and IV consists of model test cases with a great difference in measured amplitudes for the same forcing parameters. This probably occurs due to a longer or shorter duration of phase III affected by initial conditions and local breaking.

Other conclusions of physical nature are related to the effective frequency domains for swirling and other wave types as a function of the excitation amplitude. Faltinsen *et al.*[3] studied this problem theoretically and experimentally in the asymptotic limit $\delta \to 0$. These studies do not account for amplification of higher modes and damping, which are shown to be of importance in the present paper. For diagonal and lateral forcing, this leads to the following: (i) significant reduction of the effective domain of swirling relative to the asymptotic results by Faltinsen *et al.*;[3] (ii) appearance of extra zones of chaotic waves with increasing δ; and (iii) chaotic waves that may be strongly affected by initial conditions. The redistribution of the effective domains is in good agreement with model tests. Mathematical quantification of the hydrodynamic instability that depends on initial conditions should be a subject of forthcoming studies.

Other topics of interest for further studies are as follows: (i) model tests with slowly changing forcing frequency in order to detect endpoints on the steady-state response curves; (ii) estimates of damping rates for higher modes to be included into the adaptive system; (iii) nonlinear dissipation and random-like disturbances of higher modes due to local breaking and overturning; and (iv) experimental study to investigate if swirling leads to rotational flows as documented by Royon *et al.*[33] for a circular base basin.

Our theoretical model can be generalized to simultaneously include several excitation frequencies and hence be used to simulate sloshing in a ship tank in a stochastic sea described by a wave spectrum. The present studies illustrate that a large number of stochastic realizations of the sea is needed to obtain reliable information on the extreme value statistics of wave elevation and integrated hydrodynamic forces and moments on the tank. The time efficiency of our theoretical model facilitates these simulations. A shortcoming of our theory is that it does not allow for a tank roof and hence that slamming impact pressures on the tank roof cannot be predicted. The latter is of practical importance and require further studies.

APPENDIX: HYDRODYNAMIC FORCES

Let us consider small magnitude motions with translatory $\boldsymbol{v}_O=(v_{O1},v_{O2},v_{O3})$ and angular $\boldsymbol{\omega}=(\omega_1,\omega_2,\omega_3)$ velocities. These are assumed to be $O(\delta)$. Lukovsky's formula[28] gives the generic expression for the nondimensional hydrodynamic force $\boldsymbol{F}:=\boldsymbol{F}/(\mathcal{M}L_1)$ ($\mathcal{M}$ is the fluid mass) as follows:

$$\boldsymbol{F}=\boldsymbol{g}-\dot{\boldsymbol{v}}_O+\boldsymbol{\omega}\times\boldsymbol{v}_O+\boldsymbol{\omega}\times(\boldsymbol{\omega}\times\boldsymbol{r}_C)+\dot{\boldsymbol{\omega}}\times\boldsymbol{r}_C+2\boldsymbol{\omega}\times\dot{\boldsymbol{v}}_C+\ddot{\boldsymbol{v}}_C, \tag{A1}$$

where $\boldsymbol{v}_C$ is the mass center that is the function of $\{\beta_{i,j}(t), i+j\geqslant 1\}$

$$x_C=-\frac{1}{\pi^2 h}\sum_{i=1}^{\infty}\beta_{i,0}(t)\frac{1+(-1)^{i+1}}{i^2},$$

$$y_C=-\frac{1}{\pi^2 h}\sum_{i=1}^{\infty}\beta_{0,i}(t)\frac{1+(-1)^{i+1}}{i^2}, \tag{A2}$$

$$z_C = -\frac{h}{2} + \frac{1}{4h}\left(\sum_{i=1}^{\infty}\{[\beta_{i,0}(t)]^2 + [\beta_{0,i}(t)]^2\} + \frac{1}{2}\sum_{i,j=1}^{\infty}[\beta_{i,j}(t)]^2\right).$$

The generic modal system (16) is based on the relationship (15). Neglecting $o(\delta)$ simplifies (A1):

$$\boldsymbol{F} = \boldsymbol{g} - \dot{\boldsymbol{v}}_O + \dot{\boldsymbol{\omega}} \times \boldsymbol{v}_C + \ddot{\boldsymbol{v}}_C, \tag{A3}$$

where

$$\boldsymbol{g} = (g_1, g_2, g_3)^T = [g\psi_2(t), -g\psi_1(t), -g] + o(\delta) \tag{A4}$$

and

$$\dot{\boldsymbol{\omega}} \times \boldsymbol{v}_C = \begin{vmatrix} \mathbf{i} & \mathbf{j} & \mathbf{k} \\ \dot{\omega}_1 & \dot{\omega}_2 & \dot{\omega}_3 \\ 0 & 0 & -\frac{h}{2} \end{vmatrix} + o(\delta) = \left(-\frac{h}{2}\dot{\omega}_2, \frac{h}{2}\dot{\omega}_1, 0\right)^T + o(\delta). \tag{A5}$$

The roll and pitch angles ψ_1 and ψ_2 are defined in Fig. 2. Components of $\boldsymbol{F}$ are

$$F_x = g\psi_2 - \dot{v}_{O1} + \frac{h}{2}\dot{\omega}_2 - \ddot{x}_C,$$

$$F_y = -g\psi_1 - \dot{v}_{O2} - \frac{h}{2}\dot{\omega}_1 - \ddot{y}_C, \tag{A6}$$

$$F_z = -g - \dot{v}_{O3} - \ddot{z}_C.$$

[1] O. M. Faltinsen, O. F. Rognebakke, and A. N. Timokha, "Resonant three-dimensional nonlinear sloshing in a square base basin," J. Fluid Mech. **487**, 1 (2003).

[2] O. M. Faltinsen, O. F. Rognebakke, and A. N. Timokha, "Resonant three-dimensional nonlinear sloshing in a square base basin. Part 2. Effect of higher modes," J. Fluid Mech. **523**, 199 (2005).

[3] O. M. Faltinsen, O. F. Rognebakke, and A. N. Timokha, "Classification of three-dimensional nonlinear sloshing in a square-base tank with finite depth," J. Fluids Struct. **20**, 81 (2005).

[4] V. I. Stolbetsov, "On oscillations of a fluid in the tank having the shape of rectangular parallelepiped," Mekh. Zhidk. Gaza 67 (1967) (in Russian).

[5] M. Arai, L. Y. Cheng, and Y. Inoue, "3D numerical simulation of impact load due to liquid cargo sloshing," J. Soc. of Nav. Arch. of Japan **171**, 177 (1992).

[6] M. Arai, L. Y. Cheng, and Y. Inoue, "Numerical simulation of sloshing and swirling in cubic and cylindrical tank," J. Kansai Soc. Nav. Arch., Japan 97 (1993).

[7] H. N. Abramson, "The dynamics of liquids in moving containers," NASA Report, SP 106 (1966).

[8] J. W. Miles, "Resonantly forces surface waves in circular cylinder," J. Fluid Mech. **149**, 15 (1984).

[9] I. Gavrilyuk, I. A. Lukovsky, and A. N. Timokha, "A multimodal approach to nonlinear sloshing in a circular cylindrical tank," Hybrid Methods in Engineering **2**, 463 (2000).

[10] H. Ockendon, J. R. Ockendon, and D. D. Waterhouse, "Multi-mode resonance in fluids," J. Fluid Mech. **315**, 317 (1996).

[11] H. Ockendon and J. R. Ockendon, "Nonlinearity in fluid resonances," Meccanica **36**, 297 (2001).

[12] G. X. Wu, Q. W. Ma, and R. E. Taylor, "Numerical simulation of sloshing waves in 3D tank based on a finite element method," Appl. Ocean. Res. **20**, 337 (1998).

[13] Z. C. Feng and P. R. Senthna, "Symmetry-breaking bifurcations in resonant surface waves," J. Fluid Mech. **199**, 495 (1989).

[14] D. M. Henderson and J. W. Miles, "Single-mode Faraday waves in small cylinder," J. Fluid Mech. **213**, 95 (1990).

[15] J. W. Miles, "Faraday waves: rolls versus squares," J. Fluid Mech. **269**, 353 (1994).

[16] M. Perlin and W. W. Schultz, "Capillary effects on surface waves," Annu. Rev. Fluid Mech. **32**, 241 (2000).

[17] T. J. Bridges, "On secondary bifurcation of three-dimensional standing waves," SIAM J. Appl. Math. **47**, 40 (1986).

[18] T. J. Bridges, "Secondary bifurcation and change of type for three dimensional standing waves in finite depth," J. Fluid Mech. **179**, 137 (1987).

[19] P. J. Bryant and M. Stiassnie, "Different forms for nonlinear standing waves in deep water," J. Fluid Mech. **272**, 135 (1994).

[20] P. J. Bryant and M. Stiassnie, "Water waves in a deep square basin," J. Fluid Mech. **302**, 65 (1995).

[21] M. La Rocca, P. Mele, and V. Armenio, "Variational approach to the problem of sloshing in a moving container," J. Theor. Appl. Fluid Mech. **1**, 280 (1997).

[22] M. La Rocca, G. Sciortino, and M. A. Boniforti, "A fully nonlinear model for sloshing in a rotating container," Fluid Dyn. Res. **27**, 23 (2000).

[23] O. M. Faltinsen and A. N. Timokha, "Adaptive multimodal approach to nonlinear sloshing in a rectangular rank," J. Fluid Mech. **432**, 167 (2001).

[24] C. Martel, J. A. Nicolas, and J. M. Vega, "Surface-wave damping in a brimful circular cylinder," J. Fluid Mech. **360**, 213 (1998).

[25] M. Hermann and A. Timokha, "Modal modelling of the nonlinear resonant sloshing in a rectangular tank I: A single-dominant model," Math. Models Meth. Appl. Sci. **15**, 1431 (2005).

[26] T. Ikeda and R. Ibrahim, "Nonlinear random responses of a structure parametrically coupled with liquid sloshing in a cylindrical tank," J. Sound Vib. **284**, 75 (2005).

[27] M. Funakoshi and S. Inoue, "Bifurcations in resonantly forced water waves," Eur. J. Mech. B/Fluids **10**, 31 (1991).

[28] O. M. Faltinsen, O. F. Rognebakke, I. A. Lukovsky, and A. N. Timokha, "Multidimensional modal analysis of nonlinear sloshing in a rectangular tank with finite water depth," J. Fluid Mech. **407**, 201 (2000).

[29] V. E. Zakharov, "Stability of periodic waves of finite amplitude on the surface of a deep fluid," J. Appl. Mech. Tech. Phys. **2**, 190 (1968).

[30] G. H. Keulegan, "Energy dissipation in standing waves in rectangular basin," J. Fluid Mech. **6**, 33 (1959).

[31] D. H. Hill, "Transient and steady-state amplitudes of forced waves in rectangular tanks," Phys. Fluids **15**, 1576 (2003).

[32] G. I. Taylor, "An experimental study of standing waves," Proc. R. Soc. London, Ser. A **CCXVIII**, 44 (1953).

[33] A. Royon, E. J. Hopffinger, and A. Cartelier, "Nonlinear wave motions in containers and wave breaking characteristics," *Hydrodynamics VI: Theory and Applications*, edited by K. Cheng and L. Yeow (Taylor & Francis, London, 2005), pp. 555–561.